Supplementary Information (SI) for Inorganic Chemistry Frontiers.

A series of pinwheel-shaped Ln_{21}-cluster-oxo-embedded polyoxometalates as single-crystal proton-conductive and tunable photoluminescent materials

Yun Fei Cao, Xin Rong Jing, Wen-Jun Xia, Yan Qiong Sun,* Xin-Xiong Li, Shou Tian Zheng,*

Fujian Provincial Key Laboratory of Advanced Inorganic Oxygenated Materials, College of Chemistry, Fuzhou University, Fuzhou, Fujian 350108, China.

Contents1

Section S1 Experimental Methods

Materials and Instrumentation. *N,N,N',N'*-tetramethylethylenediamine, N-methylpiperazine , $Eu(NO_3)_3\cdot6H_2O$, $Gd(NO_3)_3\cdot6H_2O$, $Tb(NO_3)_3\cdot6H_2O$, $Dy(NO_3)_3\cdot6H_2O$, $NaBO_3$, Na_2SeO_3 were commercially purchased without further purification. $K_8Na_2[A\text{-}a\text{-}GeW_9O_{34}]\cdot25H_2O$ was synthesized according to the reported procedure. PXRD patterns were obtained by using an Ultima IV diffractometer with Cu-$K\alpha$ radiation (λ = 1.5418 Å) in the range 3 - 45°. Inductively coupled plasma (ICP) spectrometer analyses were conducted on an Ultima2 spectrometer. Thermal analysis was performed in a dynamic air atmosphere with a heating rate of 10 °C/min, using a NETZSCH STA 449C thermal analyzer. IR spectra were determined in the range 4000-500 cm^{-1} on a Nicolet IS50 Fourier transform infrared (FT/IR) spectrometer. The optical diffuse reflectance spectra were measured at room temperature using a Perkin-Elmer Lambda 900 Uv-vis spectrophotometer equipped with an integrating sphere attachment and $BaSO_4$ as reference. Luminescent spectra were collected with an Edinburgh Instruments FS980 TCSPC luminescence spectrometer on powdered crystal material of the compounds. The measurement of proton conductivity is carried out using alternating current impedance spectroscopy with a dual electrode configuration between 10^7 and 0.1Hz. The temperature range is 25 ~ 85 ℃, and the relative humidity (RH) range is 55~98% RH. Use the formula $\sigma = L / (RS)$ to calculate the conductivity (L, R, S represent thickness (cm), fitting resistance (Ω), and cross-sectional area (cm^2), respectively). Ac impedance measurements were carried out with a SI 1260 IMPEDANCE/GAINPHASE analyzer The relative humidity was controlled by a STIKCorp CIHI-150BS3 incubator. The samples were pressed to form a cylindrical pellet of the crystalline powder sample (~1.04 mm thickness × 5 mm ϕ) coated with C-pressed electrodes. The bulk conductivity was estimated by semicircle fittings of Nyquist plots.

Synthesis of 1-Eu: A mixture of $K_8Na_2[A\text{-}\alpha\text{-}GeW_9O_{34}]\cdot25H_2O$ (0.30 g, 0.12 mmol), $Eu(NO_3)_3$ (0.08 g, 0.18 mmol)，KCl (0.051 g, 0.68 mmol) , Na_2SeO_3 (0.055 g, 0.318 mmol), $NaBO_3$ (0.08 g, 0.98 mmol) and 4 mL of H_2O was stirred for 5 minutes in a 23 mL Teflon-lined autoclave, then 100 μL of N,N,N',N'-tetramethylethylenediamine was added, successively. The mixture was stirred for 1 hour and then heated at 140 ℃ for 3 days. The pH of the mixture before heating was 9.5, and 9.1 after cooling, showing no significant change. After cooling to room temperature and washing with mother solution, colorless bulk crystals were obtained. Yield: 100 mg (29% based on W). IR for **1-Eu** : 3367 cm^{-1} (s), 1623 cm^{-1} (m), 1365 cm^{-1} (w), 931 cm^{-1} (m), 798 cm^{-1} (s), 744 cm^{-1} (s), 696 cm^{-1} (s), 569 cm^{-1} (s).

Synthesis of 1-Gd: The preparation process of **1-Gd** is identical to **1-Eu** except that $Eu(NO_3)_3$ was replaced by $Gd(NO_3)_3$. Colorless crystals were obtained after cooling to room temperature. Yield: ca. 120 mg (31% based on W). IR for **1-Gd** : 3369 cm^{-1} (s), 1625 cm^{-1} (m), 1374 cm^{-1} (w), 931 cm^{-1} (m), 796 cm^{-1} (s), 742 cm^{-1} (s), 698 cm^{-1} (s), 570 cm^{-1} (s).

Synthesis of 1-Tb: The preparation process of **1-Tb** is identical to **1-Eu** except that $Eu(NO_3)_3$ was replaced by $Tb(NO_3)_3$. Colorless crystals were obtained after cooling to room temperature. Yield: ca. 116 mg (31% based on W). IR for **1-Tb** : 3370 cm^{-1} (s), 1623 cm^{-1} (m), 1365 cm^{-1} (w), 931 cm^{-1} (m), 798 cm^{-1} (s), 744 cm^{-1} (s), 694 cm^{-1} (s), 576 cm^{-1} (s).

Synthesis of 1-Dy: The preparation process of **1-Dy** is identical to **1-Eu** except that $Eu(NO_3)_3$ was replaced by $Dy(NO_3)_3$. Colorless crystals were obtained after cooling to room temperature. Yield: ca. 91 mg (31% based on W). IR for **1-Dy** : 3376 cm^{-1} (s), 1625 cm^{-1} (m), 1373 cm^{-1} (w), 931 cm^{-1} (m), 798 cm^{-1} (s), 744 cm^{-1} (s), 692 cm^{-1} (s), 572 cm^{-1} (s).

Synthesis of 2-Eu: A mixture of $K_8Na_2[A\text{-}\alpha\text{-}GeW_9O_{34}]\cdot25H_2O$ (0.40 g, 0.16 mmol), $Eu(NO_3)_3$ (0.06 g, 0.134 mmol)，NaCl (0.051 g, 0.87 mmol) , Na_2SeO_3 (0.051 g, 0.29 mmol) $NaBO_3$ (0.063 g, 0.77 mmol) and 4 mL of H_2O was stirred for 5 minutes in a 23 mL Teflon-lined autoclave, then 30 μL of N-methylpiperazine was added, successively. The mixture was stirred for 1 hour and then heated at 140 ℃ for 3 days. The pH of the mixture before heating was 9.8, and 8.9 after cooling, showing no significant change. After cooling to room temperature and washing with mother solution, colorless bulk crystals were obtained. Yield: 75 mg (17% based on W). IR for **2-Eu** : 3372 cm^{-1} (s), 1625 cm^{-1} (m), 1457 cm^{-1} (w), 1369 cm^{-1} (w), 1113 cm^{-1} (w), 931 cm^{-1} (m), 796 cm^{-1} (s), 740 cm^{-1} (s), 701 cm^{-1} (s), 568 cm^{-1} (s)

Synthesis of 2-Tb: The preparation process of **2-Tb** is identical to **2-Eu** except that $Eu(NO_3)_3$ was replaced by $Tb(NO_3)_3\cdot6H_2O$. Colorless crystals were obtained after cooling to room temperature. Yield: ca. 45 mg (10% based on W). IR for **2-Tb** : 3369 cm^{-1} (s), 1625 cm^{-1} (m), 1457 cm^{-1} (w), 1371 cm^{-1} (w), 1112 cm^{-1} (w), 931 cm^{-1} (m), 800 cm^{-1} (s), 740 cm^{-1} (s), 701 cm^{-1} (s), 572 cm^{-1} (s)

Single–crystal X–ray diffraction: Crystals were collected on a Bruker APEX III CCD area diffractometer equipped with a fine focus, 2.0 kW sealed tube X-ray source (MoKα radiation, λ = 0.71073 Å) operating at 150 (2) K. The empirical absorption correction was based on equivalent reflections. Structures were solved by direct methods followed by successive difference Fourier methods. Computations were performed using SHELXTL-2018/3 and final full-matrix refinements were against F^2. The contribution of disordered solvent molecules to the overall intensity data of structures was treated using the SQUEEZE method in PLATON. CCDC 2387252 (**1-Eu)** and 2387262 (**2-Eu**) contains the crystallographic data.

Single-crystal proton conductivity test: The cross-section area sizes and the length of the single crystal were 0.001 cm^2 and 0.268 cm, respectively. AC impedance measurements were carried out with a Zennium/IM6 impedance analyzer over the frequency range from 0.1 Hz to 10^7 Hz with an applied voltage of 50 mV as the temperatures were varied from 25 to 85 °C and the relative humidity (RH) was 98%. The relative humidity was controlled by a STIK Corp CIHI-150BS3 incubator. The conductivity of the samples was deduced from the Debye semicircle in the Nyquist plot. The orientation of the single crystal was determined by the Bruker D8 venture APEX5 instrument. The single-crystal measurements revealed the single-crystal shape as a hexagonal prismatic crystal, wherein the cross-section area sizes and the length were 0.001 cm^2 and 0.268 cm, respectively. Silver wires were connected to both ends of the longer axis of each crystal.

Section S2 Additional Tables

Table S1 Crystal data and structure refinement for 1-Eu and 2-Eu

Compound	**1-Eu**	**2-Eu**
Empirical formula	$H_{23}K_{30}(H_2O)_{18}\{[Ln_{21}(H_2O)_9(WO_6)(SeO_3)_6][Ln_3(SeO_3)_2]_2[(GeW_{10}O_{38})_9]\}$	$H_{27}Na_3K_{21}(H_2O)_{11}(MePIP)_2\{[Ln_{21}(H_2O)_9(WO_6)(SeO_3)_6][Ln_3(SeO_3)_2]_2[(GeW_{10}O_{38})_9]\}$
Formula weight	30265.18	33869.66
Temperature/K	150	150
Crystal system	trigonal	triclinic
Space group	$P\bar{3}c1$	$P\bar{1}$
a/Å	37.8643(19)	25.113(2)
b/Å	37.8643(19)	29.660(3)
c/Å	44.446(4)	40.083(4)
α/°	90	85.408(3)
β/	90	72.856(3)
γ/°	120	68.745(3)
Volume/Å^3	55185(7)	26577(4)
Z	4	2
ρ_{calc} g/cm^3	3.643	4.232
μ/mm^{-1}	23.349	24.226
F(000)	52164.0	30102

Compound	**1-Eu**	**2-Eu**
2θ range for data collection/°	3.73 to 50.16	3.63 to 50.14
Reflections collected	745388	814509
Independent reflections	32632 [$R_{\mathrm{int}} = 0.0843$, $R_{\mathrm{sigma}} = 0.0263$]	93847 [$R_{\mathrm{int}} = 0.0718$, $R_{\mathrm{sigma}} = 0.0369$]
Data/restraints/parameters	32632/48/1736	93847/234/5324
Data completeness	99.7%	99.5%
Goodness-of-fit on F^2	1.022	1.031
Final R indexes [I>=2σ (I)]	$R_1 = 0.0536$, $wR_2 = 0.1528$	$R_1 = 0.0594$, $wR_2 = 0.1633$
Final R indexes [all data]	$R_1 = 0.0655$, $wR_2 = 0.1644$	$R_1 = 0.0714$, $wR_2 = 0.1724$

${}^{a}R_1 = \sum||F_o|-|F_c||/\sum|F_o|$, ${}^{b}\omega R_2 = \{\sum\omega[(F_o)^2-(F_c)^2]^2/\sum\omega[(F_o)_2]^2\}^{1/2}$

Table S2. The the conductivity of 1-Eu and 2-Eu at different relative humidity (RH) and 25 ℃

Relative humidity	**1-Eu** $\sigma_1 = L/RS$ (S·cm^{-1})	**2-Eu** $\sigma_2 = L/RS$ (S·cm^{-1})
55% *RH*	1.8×10^{-3}	2.2×10^{-4}
65% *RH*	2.5×10^{-3}	3.0×10^{-4}
75% *RH*	3.5×10^{-3}	4.5×10^{-4}
85% *RH*	5.8×10^{-3}	8.9×10^{-4}
98% *RH*	1.6×10^{-2}	4.3×10^{-3}

Table S3. The temperature-dependent conductivities of compounds 1-Eu and 2-Eu at 98% RH

T (℃)	1000/T (K^{-1})	**1-Eu** $\sigma_1 = L/RS$ (S·cm^{-1})	$\mathrm{Ln}\sigma_1 T$	**2-Eu** $\sigma_2 = L/RS$ (S·cm^{-1})	$\mathrm{Ln}\sigma_2 T$
25	3.36	1.6×10^{-2}	1.59	4.3×10^{-3}	0.25
35	3.25	1.9×10^{-2}	1.74	5.7×10^{-3}	0.56
45	3.15	2.5×10^{-2}	2.08	7.7×10^{-3}	0.90
55	3.05	3.2×10^{-2}	2.34	1.0×10^{-2}	1.21
65	2.96	3.9×10^{-2}	2.57	1.3×10^{-2}	1.48
75	2.88	5.5×10^{-2}	2.94	2.0×10^{-2}	1.93
85	2.80	6.6×10^{-2}	3.17	2.3×10^{-2}	2.11

Table S4 Proton conductivities of representative POM-based conducting crystalline materials

Compounds	Conductivity$_{\mathrm{min}}$ (S cm^{-1})	Conductivity$_{\mathrm{max}}$ (S cm^{-1})	Ref

1-Eu	**1.8×10^{-3} (25 °C, 55%RH)**	**6.60×10^{-2} (85 °C, 98%RH)**	**This work**
2-Eu	**2.2×10^{-4} (25 °C, 55%RH)**	**2.30×10^{-2} (85 °C, 98%RH)**	**This work**
$H_{38}Na_{10}K_{14}(TMEDA)_8[Ln_{30}Ge_{12}W_{107}O_{420}(OH)_2(H_2O)_{14}]$·solvents	7.48×10^{-4} (25 °C, 55%RH)	1.95×10^{-2} (85 °C, 98%RH)	[1]
$H_{13}(HIm)_4K_2Na_4(H_2O)_9[Sb^{III}_9Sb^{V}Ln_3O_{14}(H_2O)_3][(SbW_9O_{33})_3(PW_9O_{34})]\cdot 26H_2O$	1.64×10^{-5} (25 °C, 55%RH)	1.64×10^{-2} (85 °C, 98%RH)	[2]
$Na_{17}K_{14}(H_2pip)_{10}H_8[La_{27}Ge_{10}W_{106}O_{406}(OH)_4(H_2O)_{24}]\cdot nH_2O$	3.8×10^{-4} (30 °C, 55%RH)	1.5×10^{-2} (85 °C, 98%RH)	[3]
$(NH_4)_{13}[Mo_{28}^{V}Mo_{126}^{VI}O_{456}H_{34}(H_2O)_{70}]Cl_{17}(ClO_4)_{14}\cdot mH_2O$	1.5×10^{-4} (22 °C, 58%RH)	1.1×10^{-2} (22 °C, 100%RH)	[4]
$Na_2[Ln_2(H_2O)_{11}]_2[Ln_3(H_2O)_3(SiW_{11}O_{39})_2]_2\cdot 69H_2O$	2.65×10^{-5} (25 °C, 55%RH)	3.54×10^{-3} (85 °C, 98%RH)	[5]
$H_9K[Cu(en)_2(H_2O)]_5[Cu(en)_2]_4[Eu(H_2O)_4]_3[Nb_{24}O_{69}(H_2O)_3]_2\cdot 2en\cdot 45H_2O$	1.57×10^{-4} (45 °C, 98%RH)	1.50×10^{-3} (85 °C, 98%RH)	[6]
$Na_4K_4(H_2pip)_6(H_2O)_{10}[Ln_{10}(OH)_2(H_2O)_{10}(GeW_{10}O_{38})_4]\cdot 29H_2O$	8.66×10^{-7} (25 °C, 55%RH)	6.35×10^{-4} (85 °C, 98%RH)	[7]
$H_9[Ln_9W_8O_{36}(H_2O)_{24}](SiW_{12}O_{40})_3\cdot 60H_2O$	9.05×10^{-7} (25 °C, 55%RH)	4.75×10^{-4} (85 °C, 98%RH)	[8]
$(TMA)_{14}H_2[Ce^{III}(H_2O)_6]\{[Ce^{IV}_7Ce^{III}_3O_6(OH)_6(CO_3)(H_2O)_{11}][(P_2W_{16}O_{59})]_3\}\cdot 41H_2O$	1.95×10^{-7} (30 °C, 98%RH)	2.65×10^{-4} (85 °C,98%RH)	[9]

Table S5 Comparison of single-crystal proton conductivity

Compounds	Conductivity (S cm^{-1})	Conditions	**Ref**
$GH\text{-}PMo_{12}$	1.90×10^{-1} [0 0 1]	85 ℃ 98% RH	[10]
$Ni_{12}Sb_{24}Si_6W_{60}$	1.11×10^{-1} [1 1 0] 1.04×10^{-1} [1 0 0] 1.53×10^{-2} [0 0 1]	85 ℃ 98% RH	[11]
$Rb_{11}Na_6H(RuW_{11}O_{38})_3$	3.84×10^{-2} $[0\ \bar{1}\ 0]$ 3.17×10^{-4} $[\bar{1}\ 1\ 1]$ 1.68×10^{-3} [1 0 1]	85 ℃ 85% RH	[12]
$[P_2Mo_5O_{23}][C_7H_7N_2]$	1.92×10^{-2} a-axis 2.42×10^{-4} b-axis 8.90×10^{-5} c-axis	50 ℃ 98% RH	[13]
1-Eu	**1.80×10^{-2} [0 0 1]** **2.20×10^{-3} [0 1 0]**	**25 ℃ 98% RH**	**This work**
$[M_6(btp)_6(H_2O)_{22}](P_2W_{18}O_{63})_3(Hbtp)_5(btp)_3$	6.39×10^{-3} [0 0 1]	85 ℃ 98% RH	[14]
PCMOF-17	1.25×10^{-3} [-1 0 1] 1.20×10^{-3} [1 1 0] 8.66×10^{-5} [0 0 1]	25 ℃ 40% RH	[15]

$[Pd(SO_3)_2]_3[Te_4(OH)_2W_6O_{28}]$	5.10×10^{-4} 1.10×10^{-4}	∥a ⊥a	25 ℃ 98% RH	[16]
$Al_{16}(P_8W_{48}O_{184})$	4.50×10^{-5}		85 ℃ 70% RH	[17]
$[H_3O][(VO_2)_3(SeO_3)_2]$	5.95×10^{-5} 1.67×10^{-5}	[1 0 0] [0 0 1]	90 ℃ 95% RH	[18]
Na-PyDat	1.04×10^{-4} 2.73×10^{-5} 4.03×10^{-6}	[1 0 0] [0 1 1] [0 1 -1]	60 ℃ 90% RH	[19]

Table S6 Inductively coupled plasma spectroscopy (ICP) analysis of 1-Eu

	Atom name	W	Ln	Se	Ge
	Calculated (%)	52.88	11.66	2.78	2.09
1-Eu	**Found (%)**	52.8	11.48	2.84	2.16

Table S7 Inductively coupled plasma spectroscopy (ICP) analysis of 1-Eu$_x$Dy$_{1-x}$

x	Eu (%)	Dy (%)	Eu+Dy (%)
1-Eu$_{0.25}$Dy$_{0.75}$	2.8	8.51	11.31
1-Eu$_{0.40}$Dy$_{0.60}$	4.62	7.22	11.84
1-Eu$_{0.60}$Dy$_{0.40}$	6.56	4.43	10.99
1-Eu$_{0.75}$Dy$_{0.25}$	7.90	2.92	10.82
1-Eu$_{0.85}$Dy$_{0.15}$	9.51	1.63	11.14

Table S8 Crystal data for 1-Eu$_x$Dy$_{1-x}$

	1-Eu	**1-Eu$_{0.85}$ Dy$_{0.15}$**	**1-Eu$_{0.75}$ Dy$_{0.25}$**	**1-Eu$_{0.60}$ Dy$_{0.40}$**	**1-Eu$_{0.40}$ Dy$_{0.60}$**	**1-Eu$_{0.25}$ Dy$_{0.75}$**
Crystal system	trigonal	trigonal	trigonal	trigonal	trigonal	trigonal
a/Å	37.8643	37.70	37.50	37.80	37.50	37.74
b/Å	37.8643	37.70	37.50	37.80	37.50	37.74
c/Å	44.446	44.76	44.58	44.90	44.54	44.86
α/°	90	90	90	90	90	90
β/	90	90	90	90	90	90
γ/°	120	120	120	120	120	120
Volume/Å^3	55185	55104	54276	55544	54251	55321

Table S9 CIE chromaticity coordinates and emitting color of **1-Eu$_x$Dy$_{1-x}$**

Samples	(x, y)	Luminescence color
1-Eu$_{0.85}$Dy$_{0.15}$	(0.62,0.33)	Red
1-Eu$_{0.75}$Dy$_{0.25}$	(0.54,0.34)	Orange-red
1-Eu$_{0.60}$Dy$_{0.40}$	(0.46,0.36)	Orange
1-Eu$_{0.40}$Dy$_{0.60}$	(0.38,0.34)	Pink
1-Eu$_{0.25}$Dy$_{0.75}$	(0.32,0.32)	White

Section S3 Additional Figures

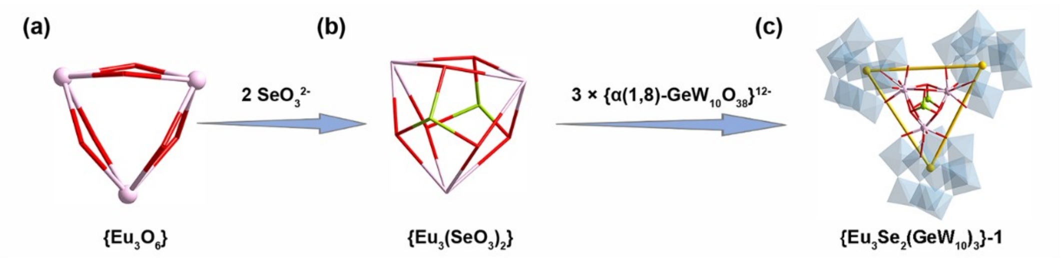

Fig. S1 View of the assembly of pinwheel-shaped {$Eu_3Se_2(GeW_{10})_3$}-1 in **1-Eu**. Color code: Se, yellow green; O, red; Eu, pink; WO_6, powder blue.

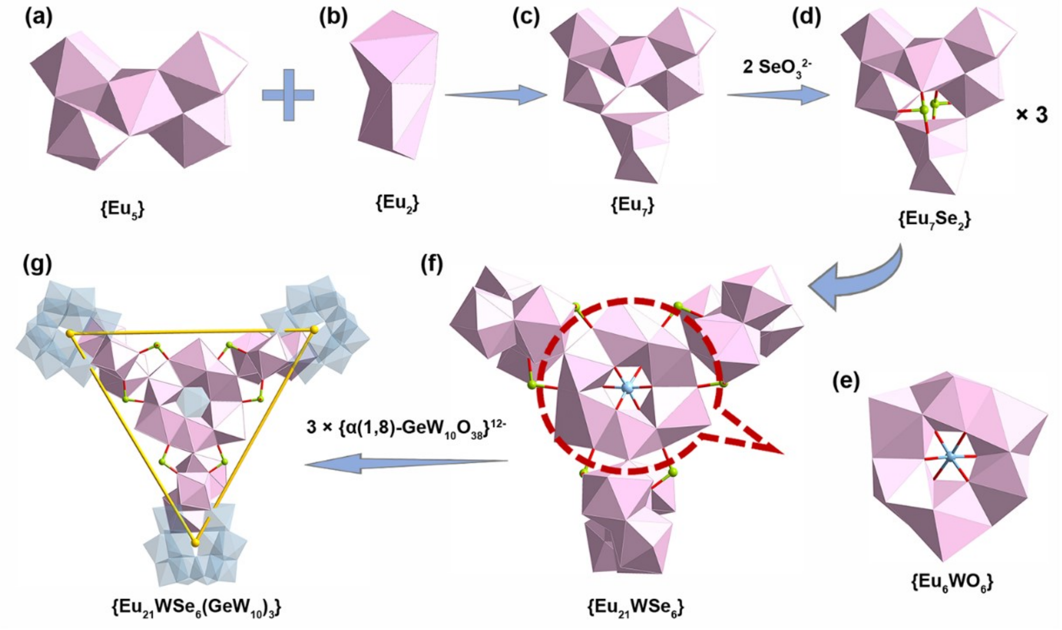

Fig. S2 View of the assembly of {$Eu_{21}Wse_6(GeW_{10})_3$}-1 in **1-Eu**: a) polyhedron representation of {Eu_5} cluster; b) {Eu_2} cluster; c) T-shaped {Eu_7} cluster; d) T-shaped {Eu_7Se_2} cluster; e) {Eu_6} ring cluster f) windmill-like {$Eu_{21}WSe_6$} cluster; g) "Y"-shaped {$Eu_{21}WSe_6(GeW_{10})_3$}-1.

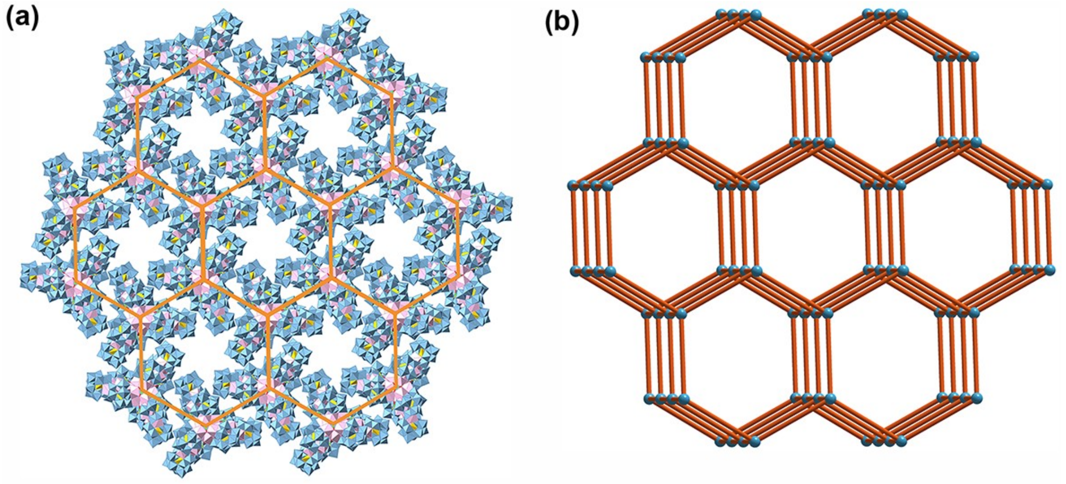

Fig. S3 (a) The 3D framework of **1-Eu** viewed along the *c*-axis, showing regular hexagonal channels; (b) 3D topology net of **1-Eu** viewed along the *c*-axis.

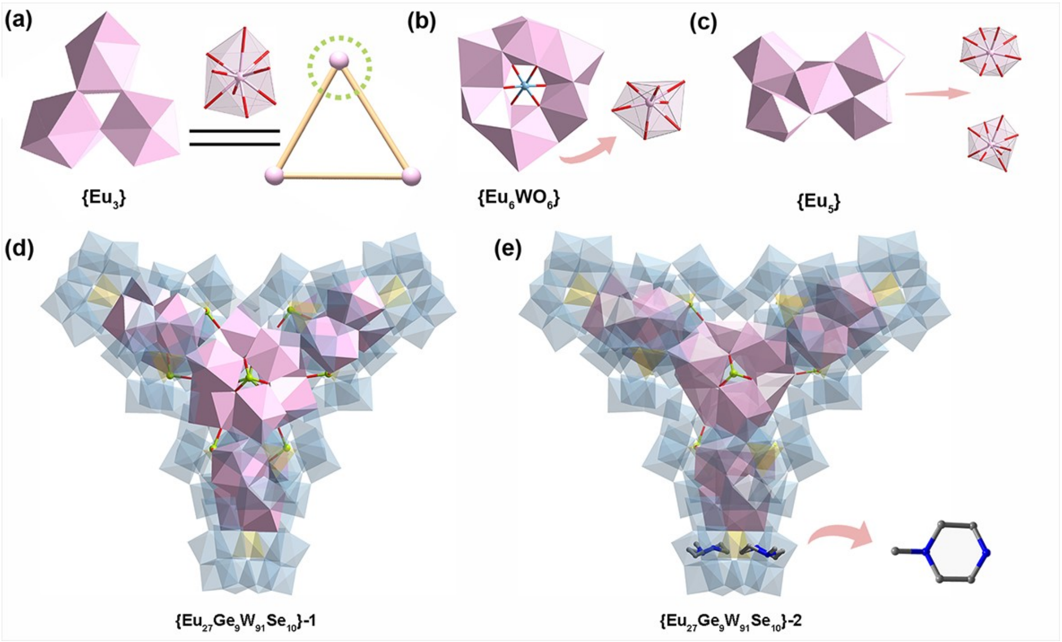

Fig. S4 (a) View of coordination environment f Eu^{3+} in $\{Eu_3O_6\}$ cluster; (b) $\{Eu_6WO_6\}$ cluster; (c) $\{Eu_5\}$ cluster; (d) polyhedron representation of **$\{Eu_{27}Se_{10}Ge_9W_{91}\}$-1** in **1-Eu**; (e) polyhedron representation of **$\{Eu_{27}Se_{10}Ge_9W_{91}\}$-2** in **2-Eu**.

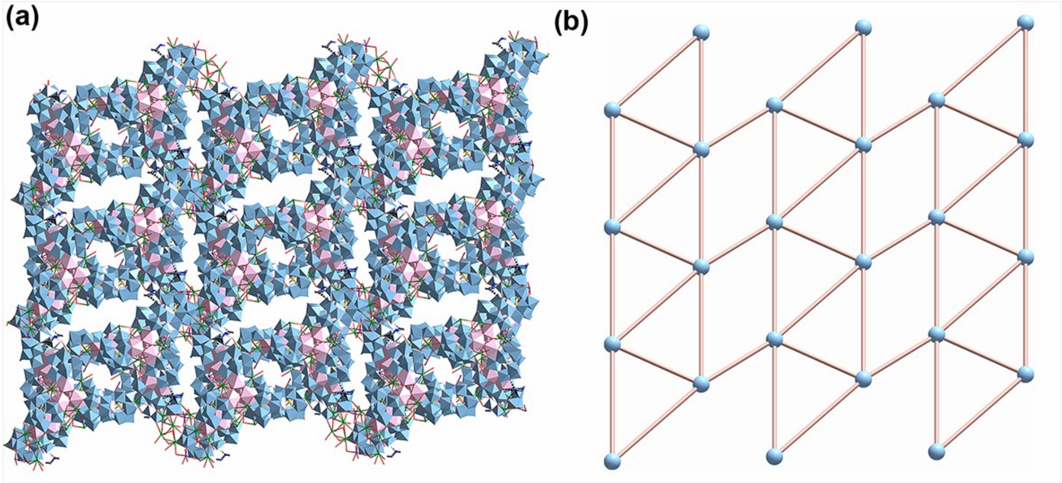

Fig. S5 (a) Packing structure of 2D layers in **2-Eu**; (b) 2D topology net of **2-Eu** viewed along the *a*-axis

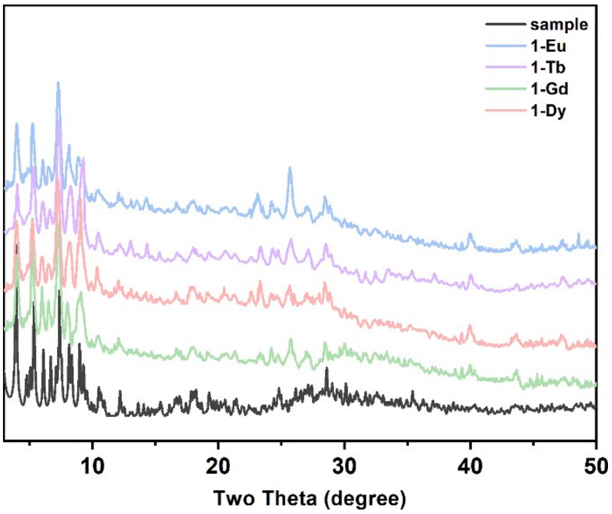

Fig. S6 PXRD patterns of **1-Ln** (Ln = Eu, Gd, Tb, Dy).

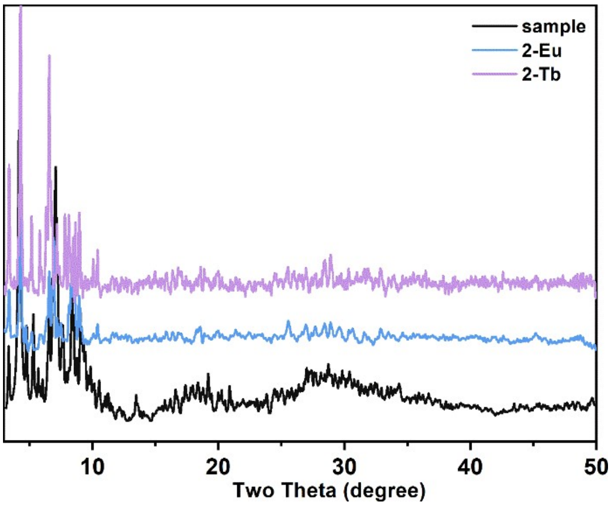

Fig. S7 PXRD pattens of **2-Ln** (Ln = Eu, Tb).

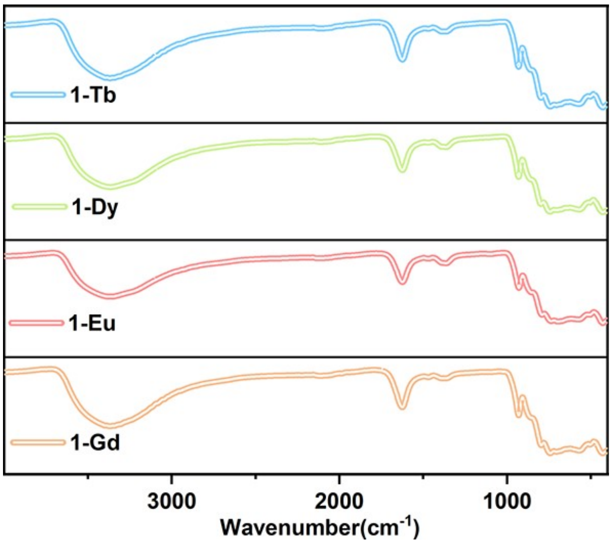

Fig. S8 (a) FT-IR spectra of **1-Ln** (Ln = Eu, Gd, Tb, Dy).

As shown in Fig, S8, the infrared spectra of **1-Ln** compounds are nearly identical, further confirming their isomorphism. The O–H stretching vibration and the H–O–H bending vibration of crystal water are observed at 3367 cm^{-1} and 1623 cm^{-1}, respectively. Characteristic peaks of **1-Ln** at 931, 798, 744, 696, and 568 cm^{-1} are assigned to the stretching vibrations of W-O$_t$, W-O$_c$-W, W–O$_b$ –W and Ge-O$_a$. The characteristic peak at 430 cm^{-1} corresponds to stretching vibrations of Ln–O$_t$.

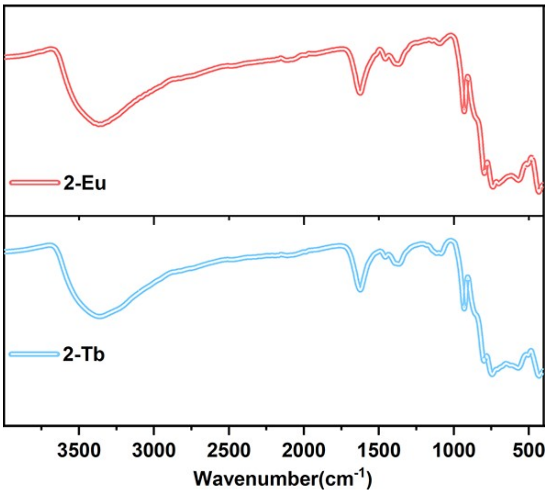

Fig. S9 (a) FT-IR spectra of **2-Ln** (Ln = Eu, Tb).

As shown in Fig, S9, the infrared spectra of **2-Ln** compounds are nearly identical, further confirming their isomorphism. The O–H stretching vibration and the H–O–H bending vibration of crystal water are observed at 3372 cm^{-1} and 1625 cm^{-1}, respectively. Characteristic peaks of **2-Ln** at 931, 796, 740, 701, and 568 cm^{-1} are assigned to the stretching vibrations of W-O$_t$, W-O$_c$-W, W–O$_b$ –W and Ge-O$_a$. The characteristic peak at 429 cm^{-1} corresponds to stretching vibrations of Ln–O$_t$.

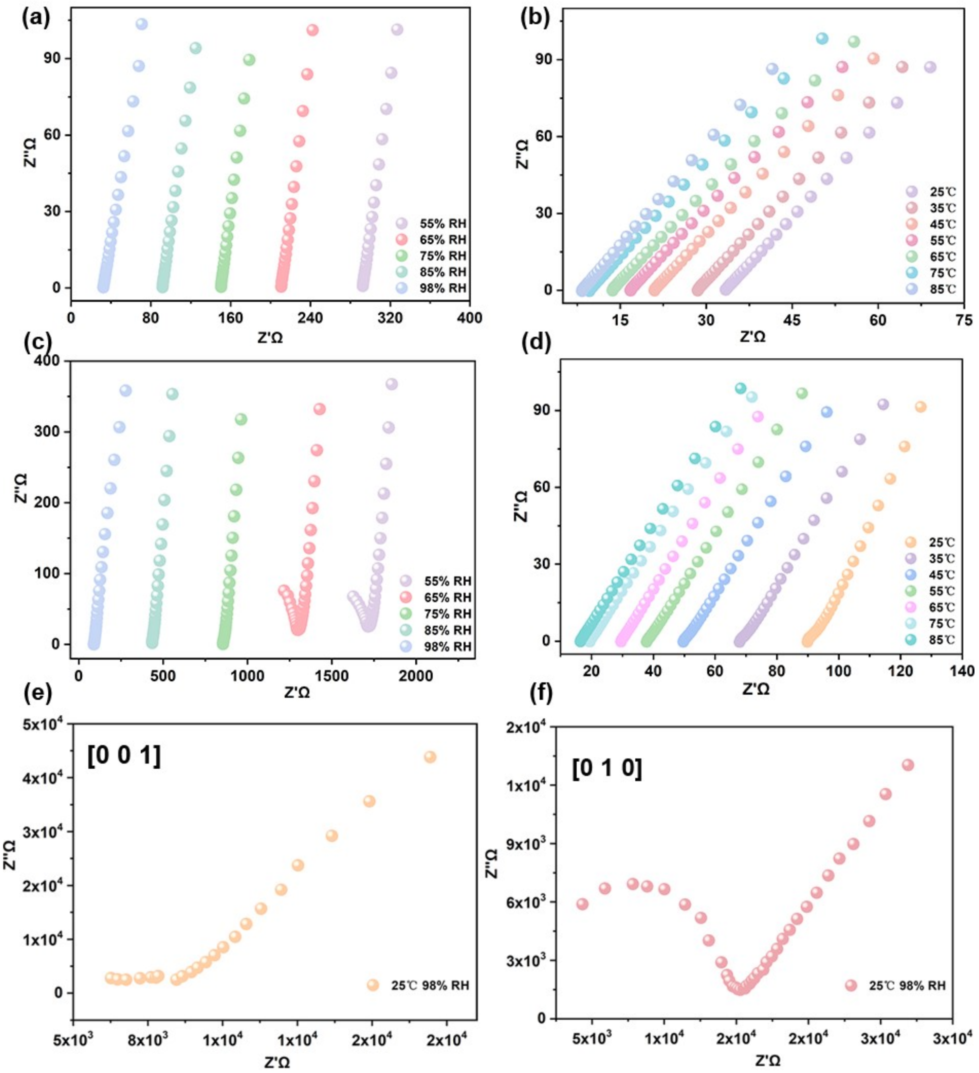

Fig. S10 Nyquist plots at 55-98% RH and 298 K for **1-Eu** (a) and **2-Eu** (c); Nyquist plots for **1-Eu** (b) and **2-Eu** (d) under different temperatures and 98% RH; (e-f) Nyquist plots for single-crystal sample of **1-Eu** along [0 0 1] and [0 1 0] directions at 98% RH and 25°C.

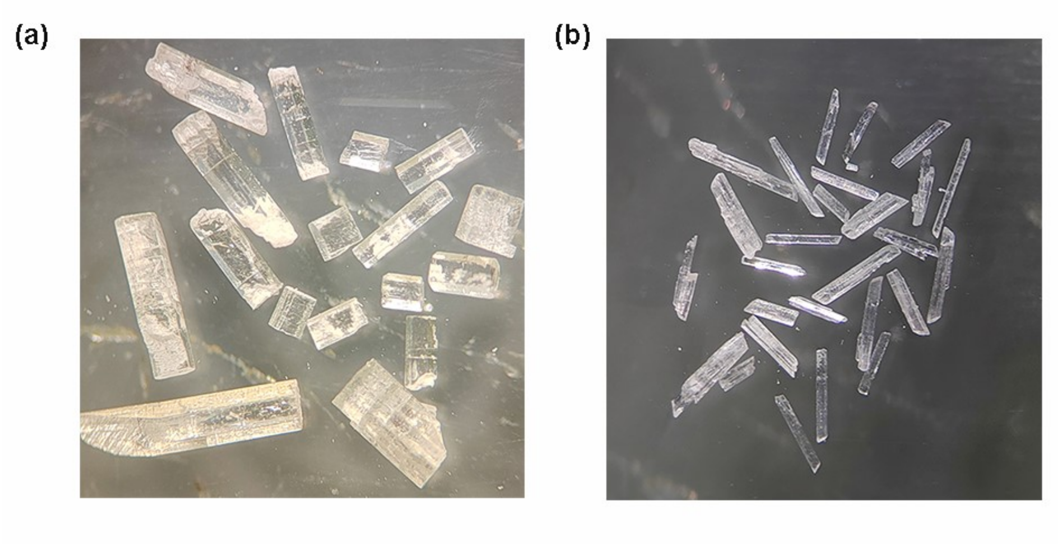

Fig. S11 The photographs of the crystal morphology of **1-Eu** and **2-Eu**.

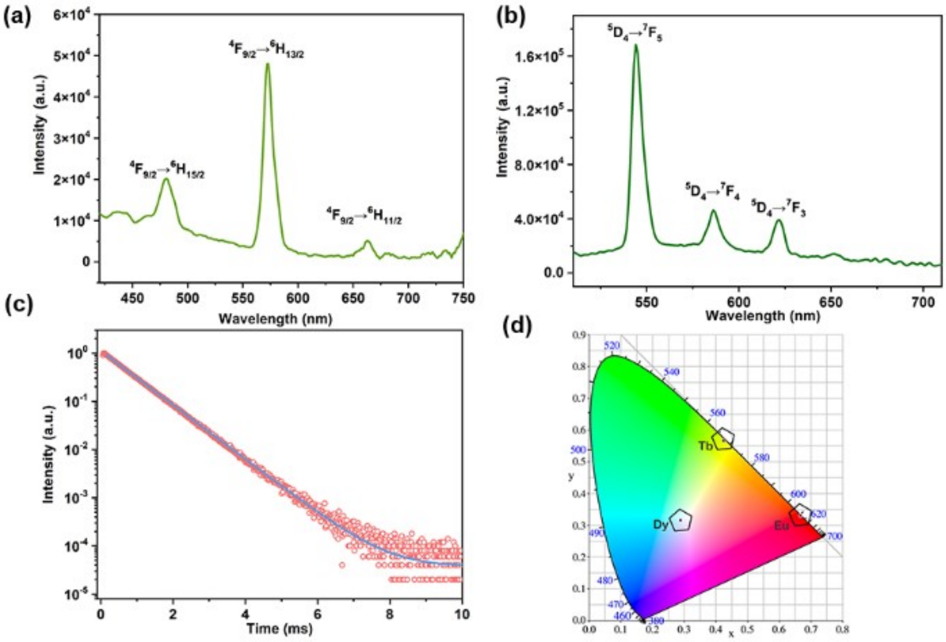

Fig. S12 (a) Room-temperature solid-state emission spectrum of **1-Dy** upon excitation at 352 nm; (b) room-temperature solid-state emission spectrum of **1-Tb** upon excitation at 485 nm; (c) luminescence decay curve of **1-Eu**; (d) CIE coordinates for **1-Eu**, **1-Dy** and **1-Tb**.

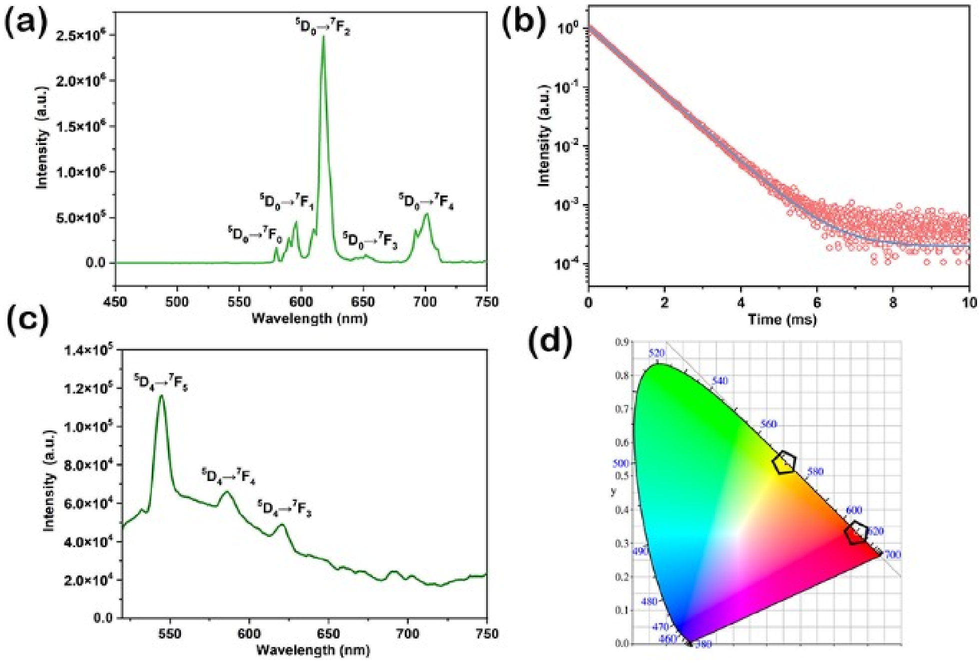

Fig. S13 (a) Room-temperature solid-state emission spectrum of **2-Eu** upon excitation at 395 nm; (b) luminescence decay curve of **2-Eu**; (c) room-temperature solid-state emission spectrum of **2-Tb** upon excitation at 485 nm; (d) CIE coordinates for **2-Eu** and **2-Tb**.

The luminescence decay curve of **2-Eu** was measured and fitted well by a single exponential function $I = A\exp(-t/\tau)$, giving a luminescent lifetime τ of 760 µs.

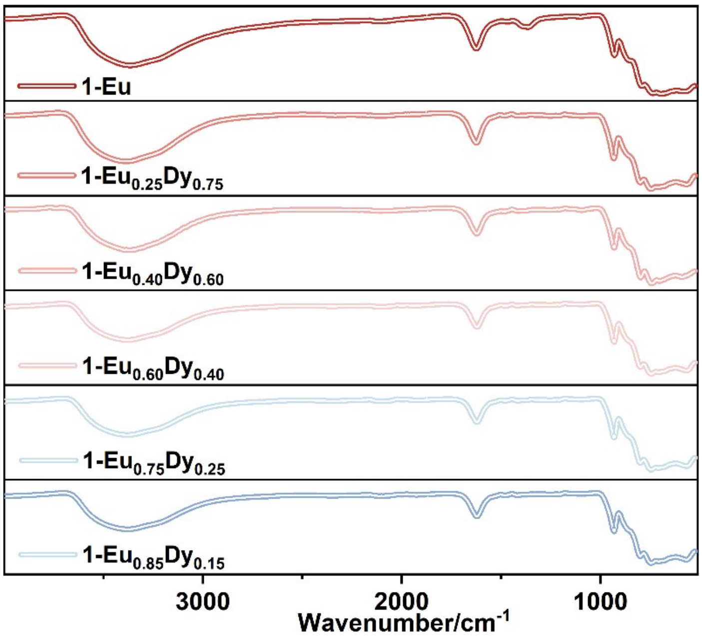

Fig. S14 (a) FT-IR spectra of **1-Eu$_x$Dy$_{1-x}$** with $0 \leq x \leq 1$.

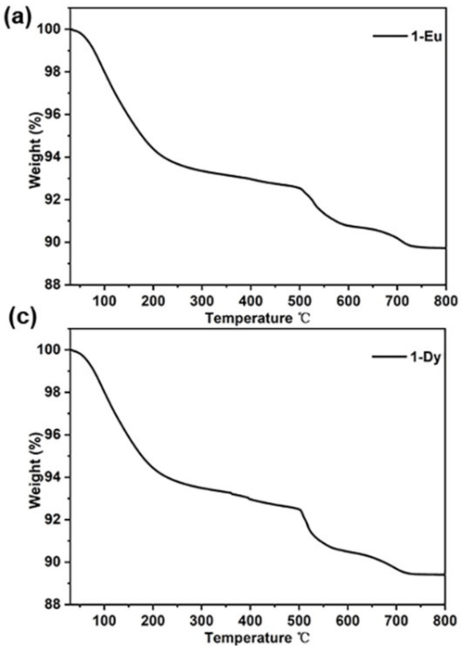

Fig. S15 TG curves of **1-Eu** (a), **1-Gd** (b), **1-Dy** (c), and **1-Tb**(d)

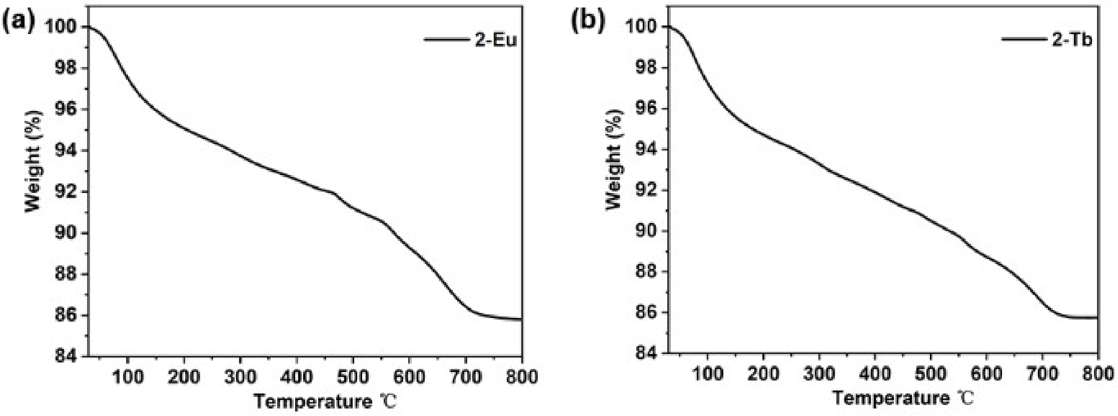

Fig. S16 TG curves of **2-Eu** (a) and **2-Tb**(d)

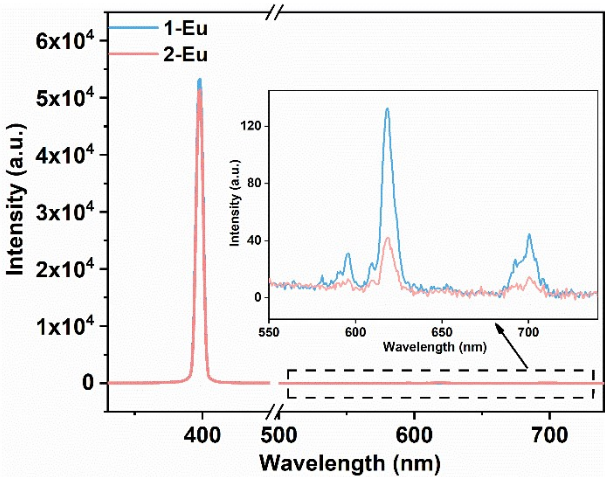

Fig. S17 The quantum yield of **1-Eu** and **2-Eu** are 26.1% and 5.9%, respectively.

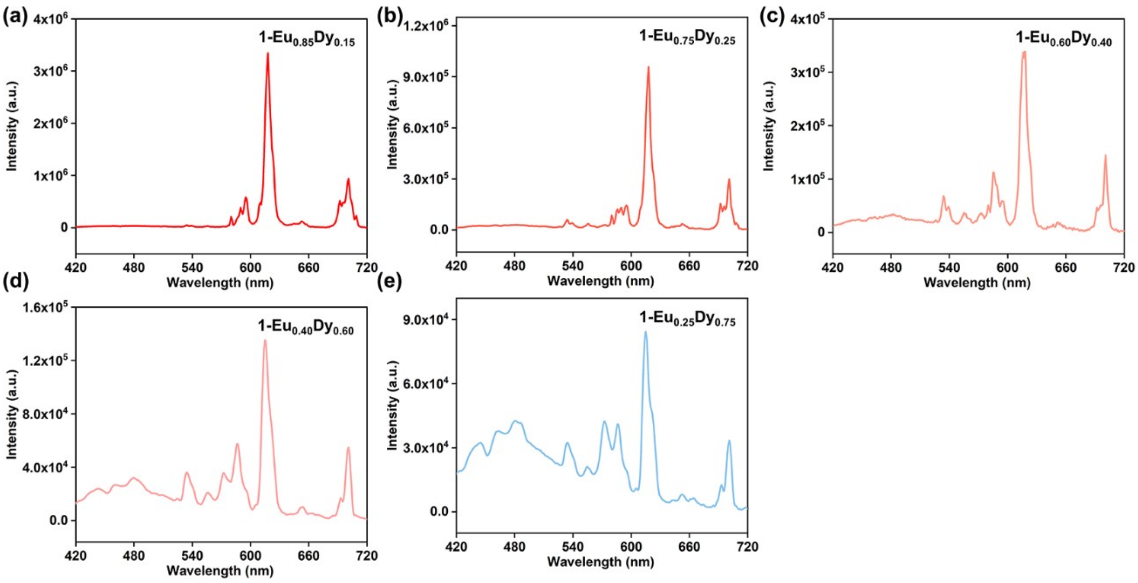

Fig. S18 Room-temperature solid-state emission spectra of **1-Eu$_x$Dy$_{1-x}$** upon excitation at 395 nm

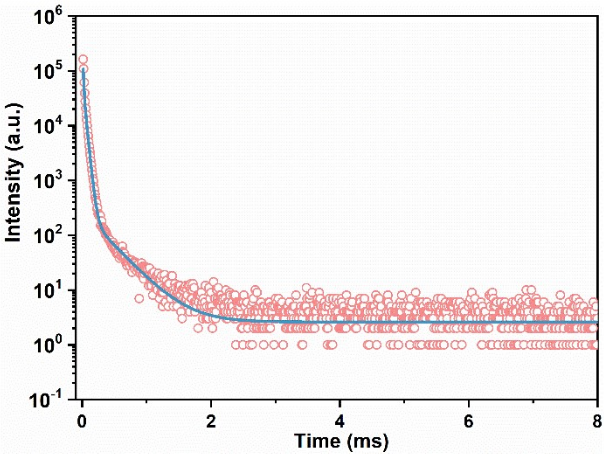

Fig. S19 Luminescence decay curve of **1-Eu$_{0.25}$Dy$_{0.75}$**

The luminescence decay curve of **1-Eu$_{0.25}$Dy$_{0.75}$** was measured and well fitted by the function as $I = A\exp(-t/\tau_1) + B\exp(-t/\tau_2) + C\exp(-t/\tau_3)$ with the luminescent lifetime τ of 33.84 μs

Section S5 References

1. Z. Li, Z.-H. Lv, H. Yu, Y.-Q. Sun, X.-X. Li and S.-T. Zheng, *CCS Chem.*, 2022, **4**, 2938-2945.

2. H.-P. Xiao, R.-T. Zhang, Z. Li, Y.-F. Xie, M. Wang, Y.-D. Ye, C. Sun, Y.-Q. Sun, X.-X. Li and S.-T. Zheng, *Inorg. Chem.*, 2021, **60**, 13718-13726.

3. Z. Li, X. X. Li, T. Yang, Z. W. Cai and S. T. Zheng, *Angew. Chem., Int. Ed.*, 2017, **56**, 2664-2669.

4. H.-Y. Wang, S.-R. Li, X. Wang, L.-S. Long, X.-J. Kong and L.-S. Zheng, *Sci. China: Chem.*, 2021, **64**, 959-963.

5. J.-H. Liu, R.-T. Zhang, J. Zhang, D. Zhao, X.-X. Li, Y.-Q. Sun and S.-T. Zheng, *Inorg. Chem.*, 2019, **58**, 14734-14740.

6. J. Zhang, R. D. Lai, Y. L. Wu, Z. K. Zhu, Y. Q. Sun, Q. X. Zeng, X. X. Li and S. T. Zheng, *Chem.*

Asian J., 2020, **15**, 1574-1579.

7. Y. Hao, L. Zhong, H.-H. Li and S.-T. Zheng, *Cryst. Growth Des.*, 2019, **19**, 1329-1335.
8. J.-H. Liu, L.-D. Lin, G.-Q. Wang, L.-Y. Li, Y.-Q. Sun, X.-X. Li and S.-T. Zheng, *Chem. Commun.*, 2020, **56**, 10305-10308.
9. P. Ma, R. Wan, Y. Wang, F. Hu, D. Zhang, J. Niu and J. Wang, *Inorg. Chem.*, 2016, **55**, 918-924.
10. M. M. Wang, J. J. Cai, H. J. Lun, M. G. Lv, J. Q. Zhang, S. Andra, B. Li, D. B. Dang, Y. Bai and Y. M. Li, *Adv. Funct. Mater.*, 2023, **34**, 2311912-2311919.
11. Y. Chen, H.-P. Wu, Z.-W. Guo, X.-X. Li, P.-W. Cai and S.-T. Zheng, *Chin. Chem. Lett.*, 2024, DOI: 10.1016/j.cclet.2024.110552.
12. M. Yang, L. Xiong, S. Ji, Y. Zhang, W. Shi, H. Li, P. Ma, J. Wang and J. Niu, *Chem. Mater.*, 2024, **36**, 8929−8935.
13. X. L. Cao, S. L. Xie, S. L. Li, L. Z. Dong, J. Liu, X. X. Liu, W. B. Wang, Z. M. Su, W. Guan and Y. Q. Lan, *Chem. - Eur. J.*, 2018, **24**, 2365-2369.
14. L.-L. Chen, Y.-Y. Wu, W.-W. Wu, M.-M. Wang, H.-J. Lun, D.-B. Dang, Y. Bai and Y.-M. Li, *Inorg. Chem.*, 2022, **61**, 8629-8633.
15. M.-Y. Zhou, H.-Y. Wang, Z.-S. Wang, X.-W. Zhang, X. Feng, L.-Y. Gao, Z.-C. Lian, R.-B. Lin and D.-D. Zhou, *Chem. Commun.*, 2022, **58**, 771-774.
16. L. Jia, Y.-X. Liu, X.-X. Li, C. Sun and S.-T. Zheng, *Inorg. Chem.*, 2024, **63**, 14308-14312.
17. P. Yang, M. Alsufyani, A. H. Emwas, C. Chen and N. M. Khashab, *Angew. Chem., Int. Ed.*, 2018, **57**, 13046-13051.
18. H.-Y. Sun, S.-H. Sun, B. Hu, L.-K. Gong, Y.-M. Zou, J.-L. Li, M.-L. Feng and X.-Y. Huang, *Inorg. Chem. Front.*, 2020, **7**, 1699-1703.
19. W.-W. Wu, J.-J. Cai, X.-Y. Liang, Z.-Z. Li, S. Andra, K. Gao, H.-J. Lun and Y.-M. Li, *ACS Appl. Mater. Interfaces*, 2024, **16**, 68358-68367.